

Mass gaps of a \mathbb{Z}_3 gauge theory with three fermion flavors in 1 + 1 dimensions

Adrien Florio ^{1,*} Andreas Weichselbaum ^{2,†} Semeon Valgushev ^{3,‡} and Robert D. Pisarski ^{1,§}

¹*Department of Physics, Brookhaven National Laboratory, Upton, NY 11973*

²*Department of Condensed Matter Physics and Materials Science,
Brookhaven National Laboratory, Upton, NY 11973-5000, USA*

³*Department of Physics and Astronomy, Iowa State University, Ames, IA, 50011, USA*

(Dated: October 30, 2023)

We consider a \mathbb{Z}_3 gauge theory coupled to three degenerate massive flavors of fermions, which we term “QZD”. The spectrum can be computed in 1 + 1 dimensions using tensor networks. In weak coupling the spectrum is that of the expected mesons and baryons, although the corrections in weak coupling are nontrivial, analogous to those of non-relativistic QED in 1 + 1 dimensions. In strong coupling, besides the usual baryon, the singlet meson is a baryon anti-baryon state. For two special values of the coupling constant, the lightest baryon is degenerate with the lightest octet meson, and the lightest singlet meson, respectively.

I. INTRODUCTION

How confinement in gauge theories produces a non-trivial mass spectrum is a problem of fundamental importance for a wide variety of problems, from Quantum ChromoDynamics (QCD) in the strong interactions [1, 2], to numerous systems in condensed matter [3].

The simplest examples of confining gauge theories are of course in the fewest number of spacetime dimensions, which is 1 + 1. The iconic examples are fermions coupled to an Abelian gauge theory, which is the Schwinger model [4–8] and N_f flavors of quarks coupled to a $SU(N_c)$ non-Abelian gauge theory, with N_c the number of colors. For $N_f \ll N_c \rightarrow \infty$, this is the ’t Hooft model [9–14].

As an Abelian theory the Schwinger model is especially useful. For a single, massless fermion, Schwinger showed that the only gauge invariant state is a single free, massive boson [4]. When the fermions are massive, however, there is an infinite number of gauge invariant pairs of fermions and anti-fermions. These obviously do not carry fermion number, and are a type of meson. When their mass is large, Coleman computed the number of mesons semi-classically [7].

While classical computers can be used to numerically compute many properties of field theories, there are some aspects — notably the evolution in real time, or theories with a sign problem — for which quantum computers are necessary. This requires controlling the Hilbert space of a field theory, which even with a lattice regularization is exponentially large. In 1+1 dimensions though, polynomial approximations have been developed, as matrix product states (MPS) efficiently represent the ground states of gapped systems [15–17]. Studies of the Schwinger model on quantum computers include Refs. [18–28]. Other properties analyzed include how mesons scatter [29, 30],

thermalization [31, 32], string breaking [20, 33–36], entanglement production in jets [37] and the dynamics in θ -vacuum [38–40].

In the massive Schwinger model the only states which survive confinement are mesons. It would be useful to study models where confinement produces states which do carry net fermion number, analogous to baryons in QCD.

There are several such models in 1 + 1 dimensions. As a $SU(N_c)$ gauge theory, the ’t Hooft model has baryons, but their properties are opaque [41–43]. A $SU(N_c)$ gauge theory coupled to N_f light flavors of quarks can be analyzed using conformal field theory, as a type of Wess-Zumino-Novikov-Witten model [44]; it behaves in a manner characteristic of such two dimensional theories. Rico *et al.* [45] studied a $SO(3)$ model in which both the quarks and the gluons lie in the adjoint representation, and so a quark and a gluon can directly combine to form a gauge invariant fermion. This is like a $SU(N_c)$ gauge theory coupled to quarks in the adjoint representation, instead of the fundamental representation as in QCD. Lastly, Farrell *et al.* [46] directly integrated out the $SU(N_c)$ gauge fields, which is possible in 1 + 1 dimensions, to obtain the mass spectrum for $SU(3)$ gauge fields coupled to two massive flavors.

While these models are all useful, we wish to study a simpler model where fermions emerge as gauge invariant states. Before doing so, it is necessary to explain in detail why in the Schwinger model, a single, massive flavor has no gauge invariant states with net fermion number. In Minkowski spacetime, the total Hamiltonian is

$$H = \int dx \left[\bar{\psi} (-i\gamma^1 \partial_1 + \gamma^1 A_1 + m) \psi \right] + \frac{g^2}{2} E^2, \quad (1)$$

where E is the electric field operator, and A_1 the conjugate gauge potential. Gauge invariance requires that we impose Gauss’s law,

$$\partial_1 E = \bar{\psi} \gamma^0 \psi. \quad (2)$$

The right hand side is just the charge density for the fermion field, which for a single flavor, is *identical* to

* aflorio@bnl.gov

† weichselbaum@bnl.gov

‡ semeonv@iastate.edu

§ pisarski@bnl.gov

the density for fermion number. (To represent Wilson loops it is necessary to add an external charge density to the right hand side, which manifestly extends the Hilbert space [47–49].) Computing the total electric charge, Q_{tot} , Gauss's law gives

$$Q_{\text{tot}} = \int dx \partial_1 E = E(\infty) - E(-\infty). \quad (3)$$

For the system to be well defined in the limit of infinite volume, we require that there is no net electric field, $E(\infty) = E(-\infty)$, and the total electric charge vanishes, $Q_{\text{tot}} = 0$. Further, since for a single flavor the total fermion number equals the total charge $N_{\text{tot}} = 0$ as well, where by N we mean the number of particles relative to half-filling, or equivalently, relative to the ground state.

Thus in a U(1) theory in $1+1$ dimensions, for a single flavor Gauss's law prevents us from introducing *any* net fermion number. In short, the global U(1) symmetry of fermion number is already part of the U(1) gauge symmetry.

This can be seen explicitly by trying to introduce a chemical potential for fermion number, μ . In the Hamiltonian formalism all thermodynamics quantities follow from the partition function,

$$Z(T, \mu) = \text{Tr} \left(e^{-(H - \mu N_{\text{tot}})/T} \right), \quad (4)$$

where the trace is over all physical states. Physical states, though, must obey Gauss's law. For U(1), this enforces $Q_{\text{tot}} = N_{\text{tot}} = 0$, and consequently, that the partition function is independent of μ , $Z(T, \mu) = Z(T, 0)$.

This can also be seen directly using the Lagrangian formalism. For a single flavor, $\mu \neq 0$ can be eliminated simply by shifting the time like component of the vector potential by an imaginary constant, $A_0 \rightarrow A_0 - i\mu/g$ [50].

With two or more flavors, then clearly one can introduce a fermion number for one flavor relative to those for the others. This is evident for two flavors, which we call up, u , and down, d . Then a net electric charge from an excess of u fermions over u anti-fermions can be precisely cancelled by an excess of down anti-fermions, \bar{d} , over d fermions. This is obviously just a chemical potential for isospin between the up and down quarks. While an isospin chemical potential exhibits interesting phenomena, such as spatially varying phases [51–53], it still leaves us bereft of gauge invariant fermions.

A simple model where there are both gauge invariant fermions and bosons was proposed in Ref. [54]. Consider a \mathbb{Z}_3 gauge theory coupled to three, degenerate massive flavors of fermions, adding strange, s , to u and d . By the Fermi exclusion principle, we cannot put two identical fermions at the same point in space, since $u^2 = 0$, *etc.* This is unlike QCD, where three quarks of the same flavor can sit on the same point in space, as long as they each carry a different color; for example, in QCD the Ω baryon is sss . Assuming that the \mathbb{Z}_3 gauge theory confines, the only way to put fermions at the same point in space is if they have different flavors. Thus the simplest singlet

under the \mathbb{Z}_3 gauge group is uds , which is like the Λ baryon in QCD.

Confinement also produces mesons in this \mathbb{Z}_3^3 theory, but these are simple to understand. Since there are three degenerate flavors, we can form \mathbb{Z}_3 singlets in two ways. There is a flavor singlet,

$$\eta' = \sum_{f=1}^3 \bar{\psi}^f \psi^f, \quad (5)$$

and a flavor octet,

$$\pi^A = \sum_{f,g=1}^3 \bar{\psi}^f t_{fg}^A \psi^g; \quad (6)$$

f and g are indices for the fundamental representation of flavor, $f, g = 1, 2, 3$, while t_{fg}^A is a SU(3) flavor matrix in the adjoint representation, $A = 1 \dots 8$. As suggested by the notation, the singlet meson is like the η' meson in QCD, while the octet multiplet π^A is analogous to the π , K , and η mesons.

Thus we have a model which has gauge invariant singlets which are both fermions (baryons) and bosons (mesons). To avoid the subtleties and complications of chiral symmetry breaking in two spacetime dimensions, we take the fermions to all have the same, nonzero mass.

In this paper we study the mass spectrum of the lightest states of this \mathbb{Z}_3^3 theory as a function of the coupling constant on the lattice. First we discuss the theory on a lattice, and how to obtain a \mathbb{Z}_3 gauge theory from the spontaneous breaking of a U(1) gauge theory. Tensor networks [55–58] and the Density Matrix Renormalization Group (DMRG) are then used to compute the mass spectrum. We find that QZD exhibits a fascinating and unexpected relation between the masses of the lightest fermions and bosons.

All states measured are gauge invariant, and so confined. This is encouraging, as there is a long history suggesting that confinement in both $2+1$ and $3+1$ dimensions are dominated by the \mathbb{Z}_3 vortices of SU(3) gauge theories [59–63]. In $1+1$ dimensions, these \mathbb{Z}_3 vortices are points in spacetime, but should also confine.

II. QZD AND ITS WEAK AND STRONG COUPLING LIMIT

Our starting point will be the following standard lattice Hamiltonian

$$H_L = -\frac{i}{2a} \sum_{x=1}^{L-1} (U_x^\dagger \chi_x^\dagger \cdot \chi_{x+1} - \text{H.c.}) - m \sum_{x=1}^L (-1)^x n_x + \frac{ag^2}{2} \sum_{x=1}^{L-1} E_x^2, \quad (7)$$

where $\chi_x \equiv (\chi_1, \dots, \chi_{N_f})_x^T$ are staggered fermions of N_f flavors that live on even/odd sites representing the original left/right chiralities. The particle number at a site

$$n_x \equiv \chi_x^\dagger \cdot \chi_x \equiv \sum_{f=1}^{N_f} \chi_x^{f\dagger} \chi_x^f, \quad (8)$$

includes a symmetric sum over all flavors. It follows from Eq. (7), that like E_x , U_x lives on the bond in between sites x and $x+1$. We consider a finite system with a total of L sites together with open boundary conditions (BC). The unit of energy is assumed in terms of the hopping amplitude $1/(2a) := 1$, i.e., $a = 1/2$, unless specified otherwise. For the remainder of the paper, we focus on the case of $N_f = 3$ fermionic flavors.

The model differs from the Schwinger model in that U_x , E_x and Gauss law implement a local \mathbb{Z}_3 algebra [64–77]. Defining the operator

$$P_x \equiv \exp\left(\frac{2\pi i}{3} E_x\right) \quad (9)$$

we impose

$$P_x^3 = U_x^3 = 1; \quad P_x^\dagger P_x = U_x^\dagger U_x = 1 \quad (10)$$

$$U_x P_x = e^{2\pi i/3} P_x U_x. \quad (11)$$

In the basis where the electric field is diagonal, U_x takes the role of a cyclic permutation operator,

$$U_x = \begin{pmatrix} 0 & 1 & 0 \\ 0 & 0 & 1 \\ 1 & 0 & 0 \end{pmatrix}, \quad (12)$$

that increments (or for U^\dagger decrements) the gauge field. This is supplemented by a \mathbb{Z}_3 Gauss law

$$P_x P_{x-1}^\dagger = \exp\left(\frac{2\pi i}{3} q_x\right). \quad (13)$$

with the charge density defined as usual for staggered fermions

$$q_x = \begin{cases} n_x & \text{for } x \text{ odd} \\ n_x - N_f & \text{for } x \text{ even} \quad (N_f = 3). \end{cases} \quad (14)$$

This permits the simple interpretation that odd sites behave like ‘particles’ which carry electrical charge $+1$, thus having $q_x = (+1)n_x$, whereas even sites behave like ‘holes’, carrying electrical charge -1 for every hole relative to completely filled, thus having $q_x = (-1)(N_f - n_x) = n_x - N_f$.

While the variables are similar to the implementation of a U(1) gauge theory by quantum links [78, 79], Gauss’ law is different, as the flux is only conserved modulo 3. We further massage Eq. (7) to make it more amenable to numerical simulations. We start by imposing open boundary conditions on our chain $E_0 = E_L = \chi_{L+1} = 0$. This allows us to use the remaining gauge transformations to remove the links U_x from the theory (see for

instance Ref. [80]) and solve Gauss’ law, expressing the electric field operators in terms of the fermionic fields. We have

$$E_x = (Q_x \bmod 3) \quad (15)$$

with the cumulative charge

$$Q_x \equiv \sum_{x' \leq x} q_{x'}, \quad (16)$$

and where modulo is taken symmetric around zero, i.e., having $E_x \in \{-1, 0, 1\}$. Thus in $1+1$ dimensions the gauge fields are not dynamical, as they can be completely determined by the charge configuration. This permits one to express a long-range Hamiltonian entirely in terms of the fermion fields. By exploiting Abelian U(1) particle number symmetry in the simulation, this is conveniently done relative to half-filling all along. With this then the symmetry label for the cumulative block particle number

$$N_x \equiv \sum_{x' \leq x} (n_{x'} - n_0), \quad (17)$$

with $n_0 = N_f/2$ the average half-filling directly specifies Q_x for even block size, i.e., $Q_x = N_x$. For odd block size this requires a minor tweak based on Eq. (14) ensuring that $Q_x \in \mathbb{Z}$.

A continuum form of a \mathbb{Z}_3 gauge theory can be constructed following Krauss, Preskill, and Wilczek [54, 81, 82]. One begins with a U(1) gauge field, coupled to fermions with unit charge, and a scalar field, ϕ , not with unit charge, but with charge *three*. Arranging the potential for the scalar field to develop an expectation value in vacuum, ϕ_0 , the photon develops a mass $m_\gamma = 3g\phi_0$, and so is screened over distances $> 1/m_\gamma$. Since the scalar field has charge three, the ϕ field is insensitive to the presence of \mathbb{Z}_3 vortices, which leaves a local \mathbb{Z}_3 symmetry, at least over distances $> 1/m_\gamma$. Remember that a scalar field has zero mass dimension in two dimensions, so by taking $\phi_0 \gg 1$, the U(1) photon is very heavy, and the theory only goes from the effective \mathbb{Z}_3 gauge symmetry, to the full U(1), at short distances $\leq 1/m_\gamma$.

Symmetries

The states in the theory can be labeled by their total particle number N_{tot} which we take relative to half-filling for convenience, and the representation of $\text{SU}(3)_f$ flavor symmetry (n_s, n_a) to which they belong. Here n_s/n_a denote the symmetric/antisymmetric rank of the representation. We then use $(N_{\text{tot}}; n_s n_a)$ as a compact notation to label all symmetry sectors, as explained in App. B. We restrict ourselves to the ground state sector $(0; 00)$, and the lightest states $(0; 11)$, $(3; 00)$, $(3; 11)$. Here $(11) \equiv \mathbf{8}$ (octet) specifies the adjoint representation of $\text{SU}(3)$. Mesons live in the $N_{\text{tot}} = 0$ sector, while baryons live in the $N_{\text{tot}} = 3$ sector. As explained in the

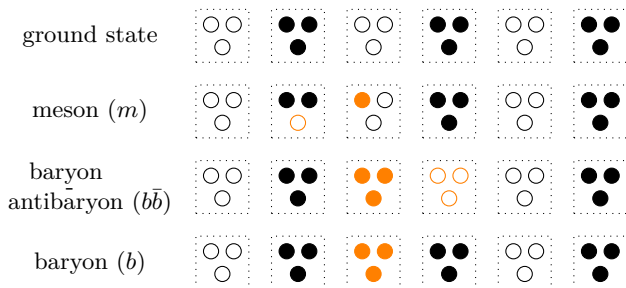


FIG. 1. Illustration of the strong coupling limit. The ground state (top row) corresponds to half-filling. The first excitation is a single baryon (last row). We highlight in orange the deviation from the ground state. The first “mesonic” state is a baryon-antibaryon pair which in QZD does not generate an electric field (by contrast, a single meson requires partial fillings; since necessarily also delocalized, by Gauss law this will always generate electric field, and hence decouple at strong coupling to large energies).

Introduction, this is unlike a $U(1)$ theory, *since both sectors can be realized in the absence of any net external charge*, i.e. in the gauge invariant sector which satisfies Gauss’s law. The ground state in the $(0;00)$ sector represents the QZD vacuum, with no baryon or meson excitations present.

III. RESULTS

A. Weak coupling regime

Naively, one might expect that the weak coupling behavior of this theory would be the usual power series in g^2 . To understand why this is not so, start first with the case of a $U(1)$ gauge theory in two spacetime dimensions. In the continuum, the Coulomb potential is

$$V(x) = g^2 \int dk \frac{e^{ikx}}{k^2} \sim g^2 |x| \quad (18)$$

is confining. For very small coupling, the fermions are heavy, and we should be able to use a non-relativistic approximation:

$$\mathcal{H}_{\text{non-rel}} = -\frac{1}{2m} \frac{d^2}{dx^2} + g^2 \frac{|x|}{4}. \quad (19)$$

Because this is a confining potential, the weak coupling expansion is not a power series in g^2/m^2 , but in $(g^2/m^2)^{1/3}$ [11–14]. In App. A we show that the meson mass behaves as

$$\frac{M_{\text{meson}}}{m} = 2m \cdot \left(1 + 0.40431 \cdot \left(\frac{g}{2m} \right)^{4/3} + O\left(\frac{g^2}{m^2} \right) \right) \quad (20)$$

B. Strong coupling regime

Another limit that is under control is the strong coupling region of the lattice model, keeping the lattice spacing a fixed as $g \rightarrow \infty$). The vacuum at infinite coupling is elementary, and direct to expand about. In terms of spins, it corresponds to half-filling: for each flavor, all even sites are occupied, while all odd sites are empty, as in Fig. 1. The first excitation is a “baryon”, with one fermion of each flavor sitting at the same site. Thanks to the periodicity of Gauss’s law for \mathbb{Z}_3 , such a configuration has zero net charge. Thus to zeroth order in $1/g$, the mass of the baryon is just $3m$, see (Fig.2 below). The leading correction in $1/g^2$ comes from the virtual hopping of a single fermion. This hopping costs ag^2 in energy, and occurs with probability $1/(4a^2)$, in $3L$ possible ways. To leading order in perturbation theory, the baryon mass is then shifted by

$$m_B = 3m + 3L \cdot \frac{1}{4a^2} \cdot \frac{1}{ag^2} = 3m + \frac{3}{4a^3} \frac{1}{g^2}. \quad (21)$$

In contrast, mesons behave very differently in strong coupling. Consider first a meson in the adjoint representation. To carry net flavor, they must be composed of a fermion on one site and an anti-fermion on an adjacent site, so unavoidably there is a nonzero electric flux connecting the two. As the energy from a single link is $\sim g^2$, adjoint mesons are very heavy at strong coupling, with a mass $\sim g^2$. Further, at $g^2 = \infty$ they are small, only a single link in size.

Somewhat unexpectedly, this is *not* true for a meson which is a flavor singlet. For a \mathbb{Z}_3 gauge theory, three fermions of different flavors, uds , are themselves a singlet under \mathbb{Z}_3 . Thus at infinite coupling, we can form a singlet meson by putting uds on one site, and $\bar{u}\bar{d}\bar{s}$ on *any* other site — no matter how far apart! At $g^2 = \infty$, then, the mass of the flavor singlet meson is just $6m$.

For large but finite coupling, the positions of the uds and $\bar{u}\bar{d}\bar{s}$ are correlated with one another, as the singlet meson mixes with three adjoint mesons. To $\sim 1/g^2$ one can show that the correction to the mass of the singlet meson is identical to that of the baryon, Eq. (21).

The size of the singlet meson is also surprising. At infinite coupling it is of *infinite* size, with the size of the singlet meson large when g^2 is large.

C. DMRG spectra

In order to access the spectrum at all couplings, we perform simulations using the Density Matrix Renormalization Group (DMRG). We take full advantage of the flavor $SU(3)_f$ global symmetry of our system by using the QSpace tensor network library [83], which is highly efficient. Utilizing this symmetry also allows us to target different symmetry sectors and gives us direct access to lowest lying excitations.

We show the spectrum in Fig. 2, for a given mass m , as a function of g^2 . We show the energy difference between the lowest lying state above the vacuum in a given symmetry sector and the vacuum, normalized by the bare mass m . The particle content of these states can be easily identified in two limits. At weak coupling, the singlet and octet states are degenerate. For $N_{\text{tot}} = 0$, they correspond to a single meson of mass $\approx 2m$. For $Q_{\text{tot}} = 3$, they correspond to a single baryon of mass $\approx 3m$. While for a baryon we can put uds on a single site and satisfy Gauss's law for the gauge group, we cannot do this for mesons. In weak coupling mesons are created by putting a fermion on one site, and an anti-fermion on another site. This implies that they create a nonzero value for \mathbb{Z}_3 electric flux. This does not matter at weak coupling as contributions to the energy from electric flux is small, a fractional power of $\sim g^2$.

Given the discussion above, the particle content of these states is easy to identify in weak and strong coupling. A meson with symmetry $(0;00)$ continuously interpolates from a single meson at weak coupling to the $b\bar{b}$ excitation at large coupling.

At weak coupling, the singlet and octet states are degenerate, with mass $2m$ at $g^2 = 0$. For $N_{\text{tot}} = 3$, there is a single baryon whose mass is $3m$ at $g^2 = 0$.

The behavior of the masses as the coupling constant increases is shown in Fig. 3. It is striking that the mass of the adjoint meson agrees well with the perturbative result of Eq. (20), which we compute only up to leading order, up to rather large coupling, certainly up to $g \sim 1$. In contrast, by $g \sim 1$ the result for the singlet meson is significantly lower than the perturbative result at leading order. This is natural because the singlet meson of QZD has no analogy in either the 't Hooft model or in QED.

At strong coupling, the first excited state in the $(0;00)$ channel corresponds to multiparticle states, including both the baryon-antibaryon ($b\bar{b}$) and states with three mesons. The dotted lines show the leading $1/g^2$ corrections, Eq. 21. There is good agreement with our numerical data.

In particular, the fact that the octet meson becomes heavy in strong coupling, and that the $(0;00)$ sector are heavier than the $(3;00)$ sector at strong coupling, indicates that there are two values of the coupling constant where there is a degeneracy between a baryon and meson state. As the coupling increases, the first is where the singlet baryon is degenerate with the octet meson. The second, at larger coupling, is where the singlet baryon and the singlet meson are degenerate. Note that this prediction is specific to \mathbb{Z}_3 , as even the singlets decouple in $U(1)$. This is illustrated in Fig. 2. These two crossings may simply be fortuitous. The second crossing, where the singlet baryon and singlet meson are degenerate, is suggestive of supersymmetry. However, we have not checked whether this degeneracy remains true for the excited states at higher mass.

The precision of our data also allows us to confirm that the theory confines. In particular, we can extract the

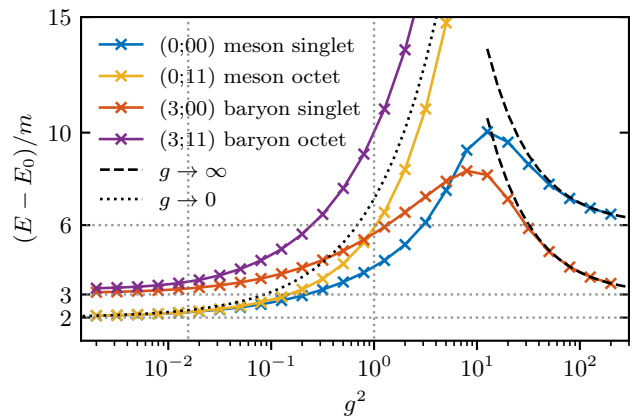


FIG. 2. Low lying excitation energies vs. coupling g^2 for mass $m = 0.125$ ($L = 120$). The red and blue lines correspond to the lowest lying $SU(3)_f$ -singlet baryons (red) and mesons (blue). Their behavior is qualitatively different from the lowest $SU(3)_f$ -octet baryon (purple) and mesons (yellow), since because of the \mathbb{Z}_3 gauge symmetry, the singlets do not decouple in the limit of strong coupling. The horizontal guides (black dashed) indicate limiting values for weak and strong coupling. The vertical guides indicate the value $g = m$ which separates weak from strong coupling, as well as $g = 1/2a = 1$ where the interaction becomes equal to the hopping amplitude (the continuum limit only has access to $g \lesssim 1$).

small coupling dependence of the mass gap. We illustrate this in Fig. 3. We plot the energy relative to the ground state minus the $g = 0$ contribution in the continuum, $\Delta_m = (E - E_0 - E_{\text{free}})/m$ with $E_{\text{free}} = 2m$ and $3m$ for mesons and baryons, respectively. A confining potential leads to non-analyticities in the coupling strength and as argued above, in an expansion in $g^{4/3}$ instead of g^2 . We show data for different masses for the singlet meson and baryons. We also show the prediction of [13] with dotted lines. For larger masses, we see strong deviations, which is completely expected as this is deeply in the lattice regime of our model $m \sim 1/a$. For smaller masses, the prediction agrees well with our data. Deviations from the $(g^2)^2/3$ at small g^2 , most prominent for mesons, can be attributed to finite-size effects.

We make this more quantitative in Fig. 4. We estimate the exponent of g by computing the logarithmic derivative of $\log(\Delta_m)$, which gives an estimate of the leading exponent at small g^2 . We first show the result for the baryon singlet (dark orange lines). The exponent converges to $(g^2)^{2/3}$ for all different masses. We can also clearly identify finite-size effects: they bend the curves away to zero, as seen by comparing the data at $m = 0.25$. The plain line corresponds to $L = 120$ while the dotted one to $L = 36$. By looking at the same quantity for the mesons, we can substantiate our claims that the finite volume effects are stronger in the sector, consistent with a smaller gap. We show in yellow the behavior of the meson octet at $m = 0.25$ for $L = 36$ and $L = 120$. The exponent still shows a strong dependence on volume

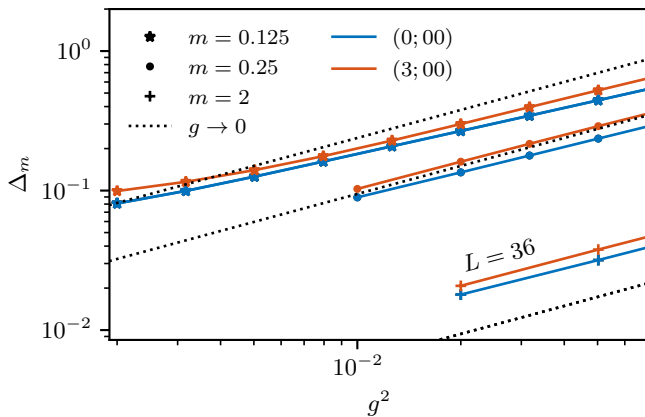


FIG. 3. Weak coupling regime ($g^2 \ll 1$) – Dependence of the gap on the coupling constant after subtracting the free case value $\Delta_m = (E - E_0 - E_{\text{free}})/m$ with $E_{\text{free}} = 2m, 3m$ for mesons and baryons, respectively. We show the meson (empty purple) and baryon (filled gray) values for different masses. The dotted lines correspond to the weak coupling $(g^2)^{2/3}$ expansion of [13]. The heavier mass is deep in the lattice regime and unsurprisingly shows large deviation. For smaller masses, the QCD₂ is surprisingly close to the \mathbb{Z}_3 data. We further discuss the remaining finite volume effects in Fig.4. The $(g^2)^{2/3}$ is a striking indication of confinement.

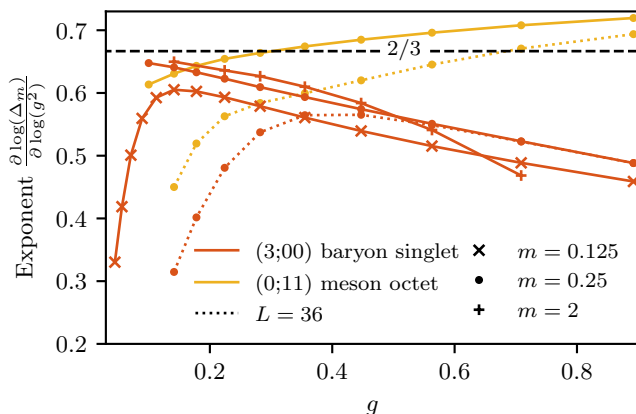


FIG. 4. Leading exponent for small g – Logarithmic derivative of data in Fig. 3. All the slopes converge to an exponent of $(g^2)^{2/3}$. The bending of the curves away from the limiting value at small g^2 signal finite volume effects in this region. This is best appreciated by comparing the dotted circle with the plain circle; they correspond to data at the same mass but different volumes.

size. The trend is however consistent with the $(g^2)^{2/3}$ expectation, confirmed in the baryon channel.

D. Topological edge modes vs. bulk excitations

Beyond the spectrum, we also study the spatial distribution of excited states. Because of staggering and open boundary conditions, the spatial structure of the ground state is non-trivial. Indeed, the use of staggered fermions in the Hamiltonian (7) gives it a simple topological nature with topologically protected edge modes at the open boundaries for the ground state. We emphasize, though, that this already also holds for the plain non-interacting model in the absence of any gauging, i.e., $g = 0$, in which case the topological aspect is known as the Su-Schrieffer-Heeger (SSH) model [84, 85]. However, at finite g this raises several non-trivial questions: (i) do the edge modes remain topologically protected when turning on finite g ? (ii) if yes, how, are these edge modes characterized in terms of excess particle number and excess electric charge? (iii) to what extent is the nature of the excited states affected by the presence of open boundaries, i.e., are the excited states true bulk modes, or rather a property of the boundary?

The edge mode in the ground state for the non-interacting case ($g = 0$) is analyzed in Fig. 5(a) at mass $m = 0.2$ for an $L = 60$ system. Clearly, the alternating onsite energy $\varepsilon_x = m(-1)^{x-1}$ directly translates to even/odd variations of the local occupations around the average filling $n_0 = 3/2$ (half-filling) throughout the system. However: this occupation pattern changes systematically towards the open boundaries. The data in Fig. 5(a) bends down at left boundary, and up at the right. The cumulative local particle number relative to half-filling, $N_x \equiv \sum_{x'=1}^x (n_{x'} - n_0)$, is shown in Fig. 5(b), in light blue in the background. As this data is still alternating around a well-defined mean value, it is averaged over even and odd lengths [darker blue for $g = 0$ in Fig. 5(b)]. This averaged data \bar{N}_x shows that the particle number offset due to the open boundary is $n_{\text{edge}} = \bar{N}_{x=L/2} = 3/4$. The precise nature of the averaging matters here: by the procedure above, $\bar{N}_x = \sum_{x'=1}^{x-1} (n_{x'} - n_0) + (n_x - n_0)/2$. If instead, for example, one had computed the cumulative particle number over unit cells which pairs up neighboring sites, the resulting excess particle number would not have been strictly universal.

Eventually, the cumulative excess particle number on the left boundary is exactly compensated at the right boundary. The cumulative total particle number offset over the entire system again returns to zero in Fig. 5(b). Therefore the excess particle number of the edge modes have the same value, but opposite signs for the two boundaries.

A non-zero interaction g increases the gap in the system, see Fig. 2. Consistently, the edge modes localize more towards each open boundary (other colored lines in Fig. 5(b)). The topological aspect of the non-interacting model remains preserved as long as the gap does not close. Conversely, the topological protection remains intact in the presence of finite gauge strength g .

The value of the fractional excess particle number can

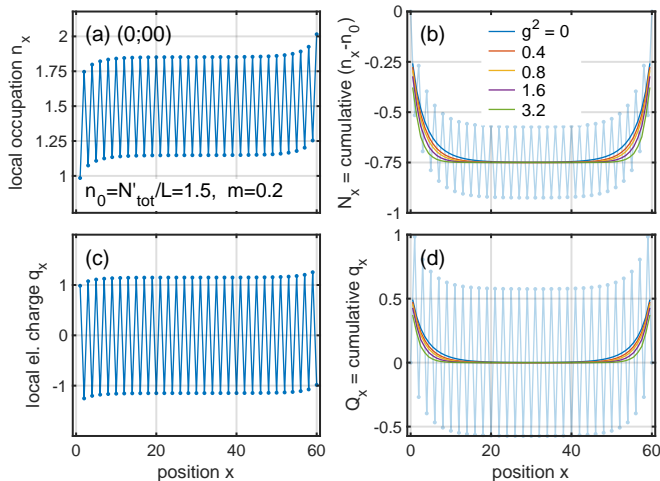


FIG. 5. Edge modes for the QZD ground state, i.e., in the symmetry sector (0;00) for a system of size $L = 60$ for $m = 0.2$ – (a) Local particle number $n_x \equiv \langle \chi_x^\dagger \cdot \chi_x \rangle$ vs. position i along the chain, for the free model $g^2 = 0$. Here $N'_{\text{tot}} \equiv \sum_x n_x$ is the actual, number of the filled Fermi sea given a finite lattice size. (b) Cumulative data in (a), after subtracting half-filling $n_0 = N_f/2 = 3/2$ for each site, i.e., plotting $N_x \equiv \sum_{i'=1}^i (n_x - n_0)$. This data (light blue) still shows alternating behavior. Averaging over even and odd x yields the smooth curve (solid darker blue). Additional averaged data for finite g is presented in different colors, where the respective value of g^2 is specified in the legend. (c) Local electric charge based on Eq. (14). (d) (Averaged) cumulative data of (c) [similar analysis as in (b), also sharing the same legend].

be motivated straightforwardly for $g \rightarrow \infty$: there one has a simple product state of alternating completely empty and filled sites [see first line (ground state) in Fig. 1]. Therefore starting from the left open boundary, the particle number relative to half-filling is given by $n_x - n_0 = [-n_0, +n_0, -n_0, +n_0, \dots]$ with $n_0 = 3/2$. Its cumulative sum is $[-n_0, 0, -n_0, 0, \dots]$. This averages to $-n_0/2$, and therefore $n_{\text{edge}} = 3/4$. This is precisely the excess number of particles observed in Fig. 5. For the extremal case here this excess particle number is strictly located right at the boundary. When reducing g , the edge mode starts to reach into the system as seen with Fig. 5(a). The cumulative excess particle number with each open boundary, nevertheless, remains pinned to precisely the same value

$$n_{\text{edge}} = \frac{3}{4} = \frac{N_f}{4}. \quad (22)$$

By having an odd number of flavors here, this shows that the edge mode carries a fractional particle number. This persists for any value of g all the way down to $g = 0$ since the gap of the system never closes. Hence as long as the system is long enough, such that the overlap of the tails of the boundary modes is negligible in the system center, one always obtains precisely the same value $\pm n_{\text{edge}}$

for the excess particle number with opposite sign for the left and right boundary. Since this includes $g = 0$, this shows that the topological protection of the SSH model remains intact also when gauging the system. Indeed, what protects SSH is inversion symmetry [86]. Gauging leaves this symmetry intact, e.g., for infinite systems or periodic systems of even length.

Now for a lattice gauge theory, by having an excess number of particles associated with an edge, one may worry that there is an electric field throughout the bulk connecting the two excess particle numbers of opposite sign for each boundary. However, this is not the case: while there is an excess number of particles due to the edge mode in the ground state, it *does not* carry any net effective electrical charge, therefore $q_{\text{edge}} = 0$.

This is demonstrated in the lower panels of Fig. 5 which repeats the same analysis as in the upper panels, but now for the electrical charge, using the number to charge conversion in Eq. (14). From the analysis in panel (d) one finds $q_{\text{edge}} = \bar{Q}_{x=L/2} = 0$. The smooth averaged curves in Fig. 5(b) simply got shifted to the zero base line in Fig. 5(d). This can be similarly motivated as for excess particle number above for the case $g \rightarrow \infty$: given the product state with alternating completely empty and filled sites, in the present case one obtains for the charge, starting from the left boundary, $q_x = [0, 0, 0, \dots]$ which averages to zero, indeed.

Having a clear understanding of the edge modes due to the open boundaries as discussed in Fig. 5, we now turn to excited states. Specifically, we want to ensure that low-energy baryon or meson excitations are true bulk excitations, and not a consequence of the presence of the open boundaries. In Fig. 6(a) we show the spatial distribution of the differential particle number occupation δn_x for the octet meson (0; 11) relative to the ground state for $g^2 = 0.4$ (same parameters as in Fig. 5). The variations throughout the entire system clearly demonstrate the bulk nature of this excitation. The cumulative sum of the variation in Fig. 6(a) is shown in Fig. 6(b), supporting a similar picture. Since the total filling remained the same as for the ground state, the data in Fig. 6(b) returns to $\delta N = 0$ for $x = L$. The variations in Fig. 6(b) diminish quickly, though, when increasing g^2 (smaller g^2 values will be analyzed in Fig. 8).

The lowest singlet baryon (b) excitation [(3;00) symmetry sector] is analyzed in Fig. 7. Analogous to the meson flavor excitation in Fig. 6, this again plots the differential variation of the particle number occupations δn_x relative to the ground state. Figure 6(a) suggests that the baryon is (weakly) attracted to the left boundary. It is still a bulk excitation, though, in the sense that its extent clearly exceeds the penetration depth of the edge mode for the same $g^2 = 0.4$ as compared to Fig. 5(b).

By adding a baryon to the system, it is free to propagate. Via the kinetic term in the Hamiltonian (hopping term), the baryon has a tendency to delocalize across the entire system. Because of the gauge field, however, this motion generates electric fields which cost energy.

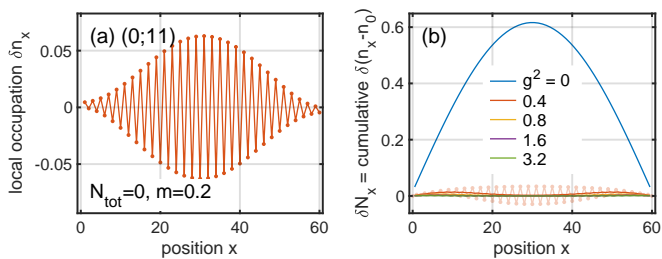


FIG. 6. Lowest octet meson excitation [lowest energy eigenstate in the (0;11) symmetry sector] – (a) Difference of local particle number δn_x relative to the ground state for $g^2 = 0.4$ [right legend also applies to panel (a); same parameters as in Fig. 5 otherwise]. (b) Cumulative data of (a) starting from the left boundary (light red) which is again even/odd averaged (solid red). Other smooth lines are obtained the same way for different g^2 as specified with the legend. Since this is a meson, eventually $\delta N_{\text{tot}} = 0$.

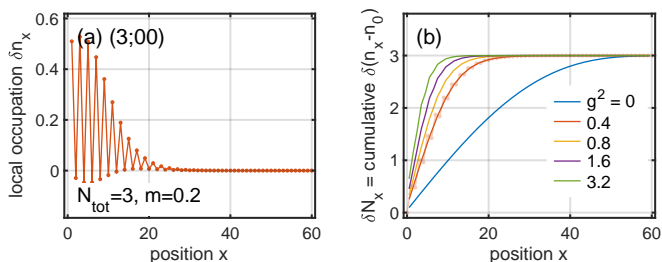


FIG. 7. Lowest baryon excitation [lowest energy eigenstate in the (3;00) symmetry sector] – same analysis as in Fig. 6 otherwise. Since this is a baryon, eventually $\delta N_{\text{tot}} = 3$.

Therefore in the presence of open boundaries, this energy is minimized by putting some of the excess particle number of $\Delta N_{\text{tot}} = 3$ right at the very first site of the left boundary as this site is particle-type: being below half-filled, this can hold more extra particles. Since there is no hopping to the left of the first site, there is less energy cost in terms of the electric field this would generate. This weak energetic bias towards the left boundary therefore is related to the convention that the system starts with particle-like site, i.e., with local energy $\varepsilon_1 = m(-1)^0 > 0$. For this reason, we expect an isolated antibaryon (\bar{b}) to be attracted to the opposite boundary at the right. From this perspective, one may expect that the meson in Fig. 6(b) for sufficiently strong g^2 starts to split a $b\bar{b}$ pair separated to opposite boundaries. This is supported by the weak double peak structure that develops in Fig. 6(b) for larger g^2 , indeed. Clear evidence for the same will be provided in Fig. 8.

It is instructive to track how excitations are distributed over a finite system with open boundaries as the interaction g is increased. Let us start by discussing the baryon excitations. As one would expect from the continuum theory, the larger the coupling strength, the more localized the baryon state can become around a perturbation

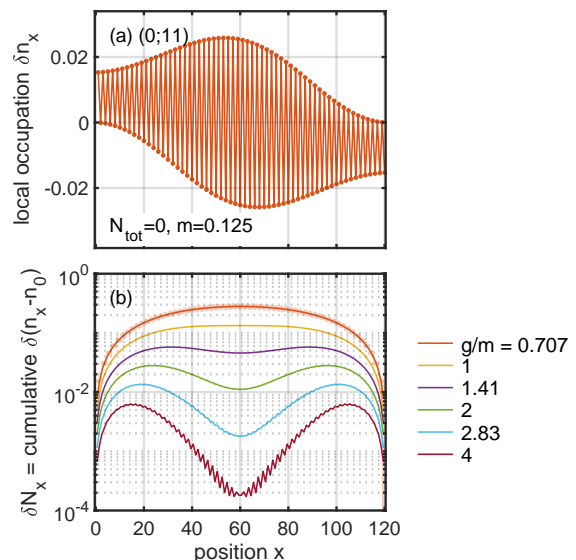


FIG. 8. Same analysis as in Fig. 6, yet for the system parameters as in Fig. 2, i.e., for twice the system size $L = 120$ here, while at the same time also smaller values of g^2 are used. Having $m = 0.125$, the legend thus implies $g^2 \leq (4m)^2 = 0.25$. The x -axis in (a) is the same as in (b), with (b) shown on semilog-y scale as compared to Fig. 6, in order to focus on the splitting of the data into a double peak structure.

of an otherwise uniform system. In the present case this perturbation is given by the abrupt end of the system due to the open boundary. We expect such localization also to carry over to the lattice model. In the extremal case $g \rightarrow \infty$ where the ground state is a simple alternating product state as depicted at the top of Fig. 1, the baryon excitation simply fills any of the particle-like sites (last row in Fig. 1). This results in degeneracy, and thus a flat-band excitation. For large but finite g , there is a weak preference on the first site (left boundary) because of the earlier argument. This more apparently still here for large g , since the QZD interaction far dominates the kinetic energy. From the QZD perspective, due to the \mathbb{Z}_3 setup an excess charge of $\delta N_x = 3$ does not generate an electric field since in that case the electric charge is effectively zero, $Q_{\text{tot}} = 0$. Hence for larger g , this confines the baryon in the neighborhood of the boundary as is seen in Fig. 7(b): the data quickly transitions from $\delta N_x = 0 \rightarrow 3$. Both, excess particle and electric charge are attracted to the left boundary. For $g \rightarrow 0$ eventually, the bias of the above type diminishes. At $g = 0$ the baryon excitation is a true bulk excitation that is symmetric around the system center [blue line in Fig. 7(b)] up to even/odd alternations.

In this light we return to the low-energy mesons. We argued with the spectra in Fig. 2 that the meson singlet [in (0;00)] starts from a single particle/hole pair at weak coupling. For strong coupling, however, this becomes a $b\bar{b}$ pair. In Fig. 1 (third line) this is exemplified locally by shifting the particles from a completely filled site to a

neighboring completely empty site.

From the present analysis we find that a single baryon is attracted to the left open boundary. By symmetry we argued that the antibaryon is attracted to the opposite boundary. Hence in the presence of $b\bar{b}$ meson at strong coupling, we expect due to the presence of the open boundaries, that the $b\bar{b}$ pair is dissociated towards the open boundaries as this permits a weak energy gain.

Revisiting Fig. 6(b), we find, indeed, that for larger g^2 a weak double peak structure develops in the data. In order to focus on this behavior, we repeat the analysis in Fig. 6(b) for the system parameters in Fig. 2 in Fig. 8 (hence twice the system length, yet also smaller g values). By specifying g in units of m in the legend of Fig. 8(b), we find that the double peak structure develops around $g \simeq m$. At close inspection, the same also holds for the parameters in Fig. 6.

Hence the appearance and dissociation of the $b\bar{b}$ meson occurs far before the peak in the data towards large g in Fig. 2: that peak in Fig. 2 is located around $g \sim 1/a$ where the coupling g becomes stronger than the one-particle bandwidth. While the latter is a pure discretization effect, the dissociation of the $b\bar{b}$ occurs much sooner around $g \sim m$. Hence this behavior is expected to be a true property of QZD also in the continuum limit. The transition towards a $b\bar{b}$ meson around $g \sim m$ thus is consistent with the intuitive notion that $g \sim m$ separates the weak from the strong coupling regime in the lattice gauge theory.

In the weak to intermediate coupling regime, the ground state (QZD vacuum) is far from the plain product state of alternating filled and empty sites as in Fig. 2, as seen for example, in Fig. 5(a). This way the QZD vacuum state acquires a non-trivial entanglement structure. Similarly, the baryon, while attracted to the boundary, has significant spatial extent. As such, from a symmetry perspective, it can assume any flavor symmetry label that derives from the combination of three particles. In terms of SU(3) symmetry sectors this also permits octets (11) aside the singlet (00) and (30) [cf. Eq. (B5)]. Hence baryons (and also antibaryons) also exist in the octet representation (11). In order to get an octet meson then, the simplest way to achieve this, is via an octet baryon with a singlet antibaryon or vice versa. Given that the octet meson splits ($b\bar{b}$) across the boundaries, the same may therefore also be expected for the simpler situation of the meson singlet.

IV. SUMMARY AND OUTLOOK

In this work, we considered “QZD”, a \mathbb{Z}_3 gauge theory with three massive flavors of fermions in 1+1 dimensions. We argued that thanks to the periodicity of Gauss’ law, it provides a unique opportunity to study “color” neutral isolated hadrons. Using state of the art tensor network simulations that take advantage of the full $U(1) \times SU(3)_f$ global symmetries, we determined the low-lying symme-

try resolved spectrum of the theory for different masses. We identified two special points, where level crossing happens between the different symmetry sectors and that most probably correspond to special theories. We then confirmed that this system is in a confining phase by verifying a striking feature of confinement in 1 + 1 dimensions: the small coupling expansion of hadrons is non analytic in g^2 , and starts at order $(g^2)^{2/3}$. We also studied the spatial distribution of the different excitations in our system. In particular, we confirmed that baryons are smaller at strong coupling. We also directly observed how the lightest meson transition from a single mesonic excitation to a pair of baryon-anti-baryon.

This work lays the ground for many potential exciting studies in 1 + 1 dimensions and beyond. A very interesting feature of this model is that, thanks to the periodicity of Gauss law, the model can be studied with a non-zero *baryon* chemical potential, in the “color” neutral sector. Studying thermodynamical quantities as a function of μ appears as an interesting outlook. The system can also be put at finite temperature. Studying properties of “color neutral” baryons can be envisaged. Extending on our analysis of how excitations are distributed in space opens the door to performing 1+1 dimensional “tomography” of hadronic states. It could in particular inform on the size dependence of baryons as a function of coupling strength. In this direction, it appears that studying the model with two light flavors and one heavier one, reducing $SU(3)_f$ to $SU(2)_f \times U(1)$ is of merit. Real-time dynamics and scattering processes can also be studied, in the ground state as well as at non-zero density. Extending the model to 2 + 1 dimensions and studying its phase diagram is also an interesting avenue. Finally, this model presents itself as a natural contender for analog as well as digital quantum computations. In 1 + 1 dimensions, it is of the same complexity as the Schwinger model but gives access to different physics. In higher-dimensions, the gauge fields do not need to be truncated and reduce the complexity burden associated to bosonic degrees of freedom.

ACKNOWLEDGMENTS

The authors would like to thank J. Barata for interesting discussions, and S. Mukherjee for discussions and for suggesting the name QZD. A.F. and R.D.P. were supported by the U.S. Department of Energy under contract DE-SC0012704 and by the U.S. Department of Energy, Office of Science, National Quantum Information Science Research Centers, Co-design Center for Quantum Advantage (C²QA), under contract number DE-SC0012704. A.W. was supported by the U.S. Department of Energy, Office of Science, Basic Energy Sciences, Materials Sciences and Engineering Division. S.V. was supported by the U.S. Department of Energy, Nuclear Physics Quantum Horizons program through the Early Career Award DE-SC0021892.

Appendix A: Weak coupling expansion

We derive here the weak coupling expansion (20) presented in the main text. The ‘‘Coulomb’’ potential is obtained by solving Gauss law for a test charge $E(x) = \frac{1}{2}\text{Sign}(x)$ and integrating. To obtain the correct small coupling expansion, it is crucial to remember we are using staggered fermion, so that the correct non-relativistic potential is obtained by integrating up to $x/2$,

$$V(x) = \frac{g^2|x|}{4}. \quad (\text{A1})$$

(Equivalently, one could rescale $g^2 \rightarrow g^2/2$ in Eq. 7.) The spectrum of the non-relativistic Hamiltonian is found by solving the associated non-relativistic Schrödinger equation [11–14]. As suggested by dimensional analysis, after rescaling $x \rightarrow y/(mg^2)^{1/3}$,

$$\left(\frac{g^4}{m}\right)^{1/3} \left(-\frac{1}{2} \frac{d^2}{dy^2} + \frac{|y|}{4}\right) \psi(y) = E_n \psi(y). \quad (\text{A2})$$

The function $\psi(y)$ are solutions to the Airy equations. Imposing continuity relations, we get

$$\psi(y) \sim \text{Ai} \left(\left(\frac{4m}{g^4}\right)^{1/3} \left(-2E_n + \frac{1}{2}g^2y\right) \right). \quad (\text{A3})$$

Valid solutions are split into symmetric and antisymmetric sectors. The symmetric sector is characterized by $\psi'(0) = 0$ and contains the lowest-lying meson. The first zero of $\text{Ai}'(-z)$ is $z \approx 1.01879$ [87], which gives Eq. (20).

This analysis is identical to that in the 't Hooft model [9, 11–14], which is a $\text{SU}(N)$ gauge theory in 1+1 dimensions as $N \rightarrow \infty$, keeping the number of quark flavors, N_f fixed. In this limit corrections to the gluon propagator from the quark loop are suppressed by $\sim N_f/N_c$, and the gluon propagator remains $= 1/k^2$ for any value of the coupling constant. In contrast, for QED in 1+1 dimensions, in general the photon propagator is modified by fermion loops. However, in weak coupling, where $g^2/m^2 \rightarrow 0$, corrections to the photon propagator from fermion loops are suppressed by $\sim (g^2/m^2)^{1/3}$, and so can be neglected.

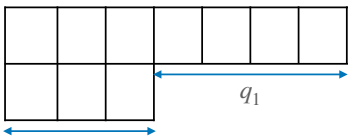
Appendix B: Symmetry labels

The Hamiltonian in Eq. (7) preserves particle number and is fully symmetric in its $N_f = 3$ fermionic flavors. Hence it has $\text{U}(1)_N \otimes \text{SU}(3)_{\text{flavor}}$ symmetry. We fully exploit these symmetries in our numerical simulations by utilizing the QSpace tensor library [83, 88, 89]. Accordingly, we can differentiate all eigenstates according to these symmetry sectors.

We specify symmetry labels in terms of the tuple of three integer values

$$q \equiv (q_0; q_1, q_2) \equiv (q_0; q_1 q_2) \quad (\text{B1})$$

where $q_0 \in \mathbb{Z}$ specifies the total number of particles relative to half-filling, and $(q_1, q_2) \equiv (q_1 q_2)$ specifies the $\text{SU}(3)$ multiplet. The latter are based on the standard multiplet labels for $\text{SU}(N)$ that directly specify the respective Young tableaux [90, 91]. This requires two labels $q_1, q_2 \geq 0$ for an $\text{SU}(3)$ multiplet which specify a Young tableaux of two rows,



$$(q_1 q_2) \equiv \begin{array}{|c|c|c|c|c|c|} \hline & & & & & \\ \hline & & & & & \\ \hline & & & & & \\ \hline & & & & & \\ \hline \end{array} \quad (\text{B2})$$

where q_1 and q_2 indicate the offset of extra boxes per row, starting from the top. This concept generalizes to general $\text{SU}(N)$ [91] with $N-1$ rows there. E.g, for $\text{SU}(2)$, $q_1 = 2S$. Completely filled columns of N boxes represent singlets and can be skipped from the tableau.

Local state space With the symmetries above, all $2^3 = 8$ states of a single site are organized into symmetry multiplets as follows: the completely filled state has symmetry labels $(3/2; 00)$, the completely empty state $(-3/2; 00)$. Half-integer particle numbers here is simply due the definition of subtracting half-filling $n_0 = 3/2$, and has no further relevance otherwise. The same also holds for blocks containing an odd number of sites. The three states with only one particle transform in the defining representation of $\text{SU}(3)$, hence represent the combined symmetry multiplet $(-1/2; 10)$. Conversely, removing a particle from the completely filled state transforms in the dual to the defining representation. Hence these states represent the symmetry multiplet $(1/2; 01)$. In their union, $1 + 1 + 3 + 3 = 8$, this exhausts the local state space.

We note that having half-integers for particle number is purely due to the definition ‘relative to half-filling’. In practice, via the tensor library QSpace [83] we use *twice* the particle number relative to half-filling, such that the symmetry label for the local particle number of a site relative to half-filling is also an integer, having $2n' \in \{-3, -1, 1, 3\}$ for a single site.

Examples for $\text{SU}(3)$ The defining representation has symmetry labels $(10) \equiv \mathbf{3}$, and its dual $(01) \equiv \bar{\mathbf{3}}$. The ‘spin’ operator transforms in the adjoint representation $(11) \equiv \mathbf{8}$ (octet),

$$\mathbf{3} \otimes \bar{\mathbf{3}} \equiv (10) \otimes (01) = (00) + (11), \quad (\text{B3})$$

with $(00) \equiv \mathbf{1}$ the scalar representation (singlet). This also represents the symmetry labels of a single particle-hole excitation (cf. meson). Note that this is completely analogous to $\text{SU}(2)$ where $\frac{1}{2} \otimes \frac{1}{2} = 0 + 1$, with $S = 1$ the $\text{SU}(2)$ spin operator.

Two particles transform in the combined space

$$\mathbf{3} \otimes \mathbf{3} \equiv (10) \otimes (10) = (20) + (01), \quad (\text{B4})$$

with $(20) \equiv \mathbf{6}$ the symmetric, and $(01) \equiv \mathbf{3}$ the antisymmetric subspace. Three particles like the baryon transform in the combined space

$$\begin{aligned} \mathbf{3} \otimes \mathbf{3} \otimes \mathbf{3} &\equiv (10) \otimes (10) \otimes (10) \\ &= (00) + (11)^2 + (30), \end{aligned} \quad (\text{B5})$$

where superscript indicates multiplicities, and $(30) \equiv \mathbf{10}$ is a fully symmetric multiplet. Dual representations are simply given by $q = (q_1 q_2) \rightarrow \bar{q} = (q_2, q_1)$. Hence all irreps with $q_1 = q_2$ are self-dual, while all others are not.

We emphasize that the specification of an irreducible representation (irrep) for $SU(N > 2)$ via the single label of its multiplet dimension only is generally insufficient because it is not unique. For example for $SU(3)$, the irreps (40) and (21) accidentally share the same multiplet dimension $d = 15$ together with their respective duals (04) and (12) .

Appendix C: DMRG convergence

We use DMRG [92, 93] in the fermionic setting where we fully exploit the $SU(3)$ flavor symmetry for the sake of numerical efficiency [83, 88, 89]. Data such as in Fig. 2 was obtained by simultaneously targeting several low energy multiplets (cf. App. B): this included 4 multiplets in $(0, 00)$, and one multiplet in each of $(\pm 3, 00)$, $(0, 11)$, and $(3, 11)$, i.e., a total of 8 multiplets, or equivalently, $6 + 2 \times 8 = 20$ states.

The bond dimension in terms of D^* multiplets was usually ramped up uniformly in an exponential way, increasing it by a factor of $2^{1/3} \sim 1.26$ for each full sweep. By keeping up to $D^* = 4,096$ multiplets, this effectively corresponded to keeping up to $D \sim 70,000$ states [Fig. 9(c)]. Thus by fully exploiting $SU(3)$ flavor symmetry, the effective bond dimension was effectively reduced by an average factor of ~ 17 by switching to a multiplet-based description. Bearing in mind, that the numerical cost of DMRG scales like $\mathcal{O}(D^3)$, this implies a gain in numerical efficiency by at least three orders of magnitude.

For the data in Fig. 2, overall, this gave rise to a discarded weight of $\delta\rho \lesssim 10^{-5}$ as shown in Fig. 9, with the entanglement entropy [Fig. 9(a)] and thus also the discarded weight largest for small g .

Appendix D: Mapping to spin Hamiltonian

In this appendix, we provide the spin-chain equivalent of Eq. (7). We obtain in using a standard Jordan-Wigner transformation and provide it only to assist the interested reader.

We introduce $3 \cdot N$ spin operators $\sigma_I^{x,y,z}$, $\sigma_I^\pm = 1/2(\sigma_I^x \pm \sigma_I^y)$, labeling them with an index $I = (n-1) \cdot 3 + f$ which uniquely maps onto indices (n, f) for the position in the lattice, n and the flavor, f . The Jordan-Wigner transformation becomes $\chi_I = \sigma_I^- \prod_{J=1}^{I-1} \sigma_J^z$, and generates the

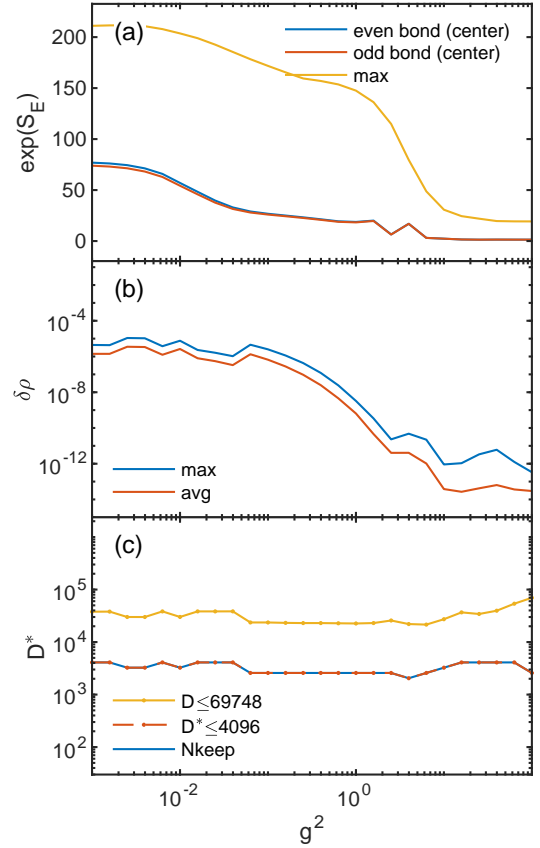


FIG. 9. DMRG convergence analysis for the data in Fig. 2 vs. QZ3 coupling g^2 (having $m = 0.125$, $L = 120$). In the simulations a total of 8 multiplets was targeted simultaneously: 4 multiplets in $(0, 00)$, and one multiplet in each of $(\pm 3, 00)$, $(0, 11)$, and $(3, 11)$, corresponding to a total of $6 + 2 \times 8 = 20$ states. (a) Exponentiated block entanglement entropy in the system center, and also the overall maximum along chain (the entanglement profile is strongly asymmetric around the system center, because multiple states are targeted). (b) Minimum and average discarded weight for last 2-site DMRG sweep. (c) DMRG bond dimension in last sweep, keeping up to $N_{\text{keep}} = D^* \leq 4,096$ multiplets (corresponding up to $D \leq 69,748$ states).

spin Hamiltonian

$$\begin{aligned} H &= \sum_{n=1}^N \sum_{f=1}^3 \left(-\frac{i}{2a} \sigma_{n,f}^+ \sigma_{n+1,f}^- S_{n,f}^{n+1,f} + \text{h.c.} \right) \\ &+ \sum_{x=n}^N \sum_{f=1}^3 \left(\frac{m}{2} (-1)^n \sigma_{n,f}^z \right) \\ &+ \frac{g^2}{2} \sum_{n=1}^N \left(\frac{2\pi}{3} \sum_{l=1}^n \left(\left(\frac{\sigma_{n,f}^z}{2} + \frac{(-1)^n}{2} \right) \bmod 3 \right) \right)^2, \end{aligned} \quad (\text{D1})$$

where $S_{n,f}^{n+1,f} = \prod_{J=3n-3+f}^{3n+f} \sigma_J^z$ is a string of $\sigma_{n,f}^z$ operators arising from the multi-flavor Jordan-Wigner transform. Similar strings arise in mapping a $SU(3)$ gauge

theory in $1 + 1$ dimensions onto spin variables [46].

Appendix E: Nonzero chemical potential

We present in this appendix exploratory results of QZD at non-zero baryon chemical potential. They are of value for this work as they provide a completely independent determination of the baryon mass and provide a convincing cross-check of our numerical analysis. For context, the behavior of QCD at low temperatures and chemical potential is directly relevant to the collision of heavy ions at moderate energies [94] and to the behavior of neutron stars as observed by multimessenger astronomy [95]. At non-zero quark chemical potential μ_{qk} the quark determinant in the Euclidean action is complex, and so direct numerical simulations using importance sampling are not possible. When $\mu_{\text{qk}} < T$, thermodynamics quantities can be computed in several ways, including: expanding in a Taylor series in μ_{qk} [96–100]; analytic continuation from imaginary chemical potential [101–104]; reweighting techniques [105, 106]; strong coupling expansions [107–113]; complex Langevin equations [114–117]; approximate solutions of the Schwinger-Dyson equations [118–120]; and the functional renormalization group [121–130].

As a first step we consider QZD at $\mu \neq 0$, finding the ground state of

$$H_\mu = H_0 - \mu \sum_x n_x, \quad (\text{E1})$$

as a function of μ , with H_0 the Hamiltonian in Eq. (1). For this simulation we had used the package ITensor [131, 132] without imposing any symmetry constraint. In this DMRG simulation we kept up to 600 states.

In Fig. 10 we show the expectation value of the particle number as a function of μ . It vanishes until $\mu = m_{(3,00)}$, where $m_{(3,00)}$ is the mass of the lightest baryon. It is then constant until it jumps again, to various multiples of three. That the number density vanishes until $\mu > m_{(3,00)}$ illustrates "silver blaze" phenomenon [133, 134]: the ground state at $\mu = 0$ remains the ground state of the grand canonical ensemble until the chemical potential exceeds the mass of the lightest state which

carries fermion number. It is an important consistency check that $m_{(3,00)}$ determined from the silver blaze phenomenon agrees with the direct calculation in Sec. III C. That the number density only jumps to multiples of three follows from gauge invariance under the local \mathbb{Z}_3 symmetry: baryons always carry u , d , and s fermions in common multiples. This is in contrast to a $U(1)$ gauge theory, where as we showed in the Sec. I, Gauss's law excludes a nonzero value for the electric charge, or fermion number. As $L \rightarrow \infty$, Fig. 10 would be a smooth curve, with N/L a smoothly varying function. For finite L , however, this is a series of steps that increases in multiples of three, thus guaranteeing a well-defined baryon number. The absence of some multiples of three is an artifact due to our resolution in μ . Note also that the fact the first plateau is

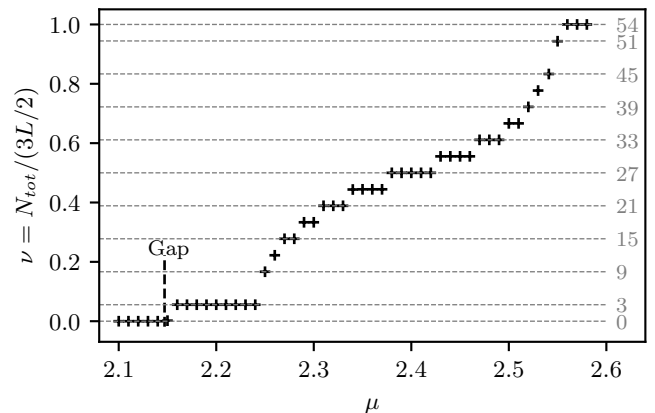


FIG. 10. The total number of particles as a function of the chemical potential, for $m = 2$, $L = 36$ and $g^2 = 1.466$. The vertical axis is scaled such that $\nu = 1$ is a completely filled system.

larger than the other can probably be attributed to the open boundary as discussed with Fig. 7 in the main text.

A more detailed study at finite chemical potential is left for future work.

-
- [1] Kenneth G. Wilson, "Confinement of Quarks," *Phys. Rev. D* **10**, 2445–2459 (1974).
 - [2] John B. Kogut and Leonard Susskind, "Vacuum Polarization and the Absence of Free Quarks in Four-Dimensions," *Phys. Rev. D* **9**, 3501–3512 (1974).
 - [3] Eduardo H. Fradkin, *Field Theories of Condensed Matter Physics*, Vol. 82 (Cambridge Univ. Press, Cambridge, UK, 2013).
 - [4] Julian S. Schwinger, "Gauge Invariance and Mass. 2." *Phys. Rev.* **128**, 2425–2429 (1962).
 - [5] Tom Banks, Leonard Susskind, and John B. Kogut, "Strong Coupling Calculations of Lattice Gauge Theories: (1+1)-Dimensional Exercises," *Phys. Rev. D* **13**, 1043 (1976).
 - [6] Sidney R. Coleman, R. Jackiw, and Leonard Susskind, "Charge Shielding and Quark Confinement in the Massive Schwinger Model," *Annals Phys.* **93**, 267 (1975).
 - [7] Sidney R. Coleman, "More About the Massive Schwinger Model," *Annals Phys.* **101**, 239 (1976).
 - [8] N. S. Manton, "The Schwinger Model and Its Axial Anomaly," *Annals Phys.* **159**, 220–251 (1985).
 - [9] Gerard 't Hooft, "A Two-Dimensional Model for Mesons," *Nucl. Phys. B* **75**, 461–470 (1974).

- [10] Curtis G. Callan, Jr., Nigel Coote, and David J. Gross, “Two-Dimensional Yang-Mills Theory: A Model of Quark Confinement,” *Phys. Rev. D* **13**, 1649 (1976).
- [11] Pedro Fonseca and Alexander Zamolodchikov, “Ising spectroscopy. I. Mesons at $T < T(c)$,” (2006), arXiv:hep-th/0612304.
- [12] V. A. Fateev, S. L. Lukyanov, and A. B. Zamolodchikov, “On mass spectrum in ’t Hooft’s 2D model of mesons,” *J. Phys. A* **42**, 304012 (2009), arXiv:0905.2280 [hep-th].
- [13] Iskander Ziyatdinov, “Asymptotic properties of mass spectrum in ’t Hooft’s model of mesons,” *Int. J. Mod. Phys. A* **25**, 3899–3910 (2010), arXiv:1003.4304 [hep-th].
- [14] R. A. Zubov, S. A. Paston, and E. V. Prokhvatilov, “Exact solution of the ’t Hooft equation in the limit of heavy quarks with unequal masses,” *Theor. Math. Phys.* **184**, 1281–1286 (2015).
- [15] Boye Buyens, Jutho Haegeman, Karel Van Acoleyen, Henri Verschelde, and Frank Verstraete, “Matrix product states for gauge field theories,” *Phys. Rev. Lett.* **113**, 091601 (2014), arXiv:1312.6654 [hep-lat].
- [16] M. C. Bañuls, K. Cichy, K. Jansen, and J. I. Cirac, “The mass spectrum of the Schwinger model with Matrix Product States,” *JHEP* **11**, 158 (2013), arXiv:1305.3765 [hep-lat].
- [17] J. Ignacio Cirac, David Perez-Garcia, Norbert Schuch, and Frank Verstraete, “Matrix product states and projected entangled pair states: Concepts, symmetries, theorems,” *Rev. Mod. Phys.* **93**, 045003 (2021), arXiv:2011.12127 [quant-ph].
- [18] Philipp Hauke, David Marcos, Marcello Dalmonte, and Peter Zoller, “Quantum simulation of a lattice Schwinger model in a chain of trapped ions,” *Phys. Rev. X* **3**, 041018 (2013), arXiv:1306.2162 [cond-mat.quant-gas].
- [19] E. Rico, T. Pichler, M. Dalmonte, P. Zoller, and S. Montangero, “Tensor networks for Lattice Gauge Theories and Atomic Quantum Simulation,” *Phys. Rev. Lett.* **112**, 201601 (2014), arXiv:1312.3127 [cond-mat.quant-gas].
- [20] T. Pichler, M. Dalmonte, E. Rico, P. Zoller, and S. Montangero, “Real-time Dynamics in U(1) Lattice Gauge Theories with Tensor Networks,” *Phys. Rev. X* **6**, 011023 (2016), arXiv:1505.04440 [cond-mat.quant-gas].
- [21] Erez Zohar, J. Ignacio Cirac, and Benni Reznik, “Quantum Simulations of Lattice Gauge Theories using Ultracold Atoms in Optical Lattices,” *Rept. Prog. Phys.* **79**, 014401 (2016), arXiv:1503.02312 [quant-ph].
- [22] E. A. Martinez et al., “Real-time dynamics of lattice gauge theories with a few-qubit quantum computer,” *Nature* **534**, 516–519 (2016), arXiv:1605.04570 [quant-ph].
- [23] Christine Muschik, Markus Heyl, Esteban Martinez, Thomas Monz, Philipp Schindler, Berit Vogell, Marcello Dalmonte, Philipp Hauke, Rainer Blatt, and Peter Zoller, “U(1) Wilson lattice gauge theories in digital quantum simulators,” *New J. Phys.* **19**, 103020 (2017), arXiv:1612.08653 [quant-ph].
- [24] N. Klco, E. F. Dumitrescu, A. J. McCaskey, T. D. Morris, R. C. Pooser, M. Sanz, E. Solano, P. Lougovski, and M. J. Savage, “Quantum-classical computation of Schwinger model dynamics using quantum computers,” *Phys. Rev. A* **98**, 032331 (2018), arXiv:1803.03326 [quant-ph].
- [25] M. C. Bañuls et al., “Simulating Lattice Gauge Theories within Quantum Technologies,” *Eur. Phys. J. D* **74**, 165 (2020), arXiv:1911.00003 [quant-ph].
- [26] Federica M. Surace, Paolo P. Mazza, Giuliano Giudici, Alessio Lerose, Andrea Gambassi, and Marcello Dalmonte, “Lattice gauge theories and string dynamics in Rydberg atom quantum simulators,” *Phys. Rev. X* **10**, 021041 (2020), arXiv:1902.09551 [cond-mat.quant-gas].
- [27] Mari Carmen Bañuls and Krzysztof Cichy, “Review on Novel Methods for Lattice Gauge Theories,” *Rept. Prog. Phys.* **83**, 024401 (2020), arXiv:1910.00257 [hep-lat].
- [28] Bing Yang, Hui Sun, Robert Ott, Han-Yi Wang, Torsten V. Zache, Jad C. Halimeh, Zhen-Sheng Yuan, Philipp Hauke, and Jian-Wei Pan, “Observation of gauge invariance in a 71-site Bose–Hubbard quantum simulator,” *Nature* **587**, 392–396 (2020), arXiv:2003.08945 [cond-mat.quant-gas].
- [29] Marco Rigobello, Simone Notarnicola, Giuseppe Magnifico, and Simone Montangero, “Entanglement generation in (1+1)D QED scattering processes,” *Phys. Rev. D* **104**, 114501 (2021), arXiv:2105.03445 [hep-lat].
- [30] Marco Rigobello, Giuseppe Magnifico, Pietro Silvi, and Simone Montangero, “Hadrons in (1+1)D Hamiltonian hardcore lattice QCD,” (2023), arXiv:2308.04488 [hep-lat].
- [31] Jean-Yves Desaulles, Debasish Banerjee, Ana Hudomal, Zlatko Papić, Arnab Sen, and Jad C. Halimeh, “Weak ergodicity breaking in the Schwinger model,” *Phys. Rev. B* **107**, L201105 (2023), arXiv:2203.08830 [cond-mat.str-el].
- [32] Titas Chanda, Jakub Zakrzewski, Maciej Lewenstein, and Luca Tagliacozzo, “Confinement and lack of thermalization after quenches in the bosonic Schwinger model,” *Phys. Rev. Lett.* **124**, 180602 (2020), arXiv:1909.12657 [cond-mat.stat-mech].
- [33] Stefan Kühn, Erez Zohar, J. Ignacio Cirac, and Mari Carmen Bañuls, “Non-Abelian string breaking phenomena with Matrix Product States,” *JHEP* **07**, 130 (2015), arXiv:1505.04441 [hep-lat].
- [34] Giuseppe Magnifico, Marcello Dalmonte, Paolo Facchi, Saverio Pascazio, Francesco V. Pepe, and Elisa Ercolessi, “Real Time Dynamics and Confinement in the \mathbb{Z}_n Schwinger-Weyl lattice model for 1+1 QED,” *Quantum* **4**, 281 (2020), arXiv:1909.04821 [quant-ph].
- [35] Wibe A. de Jong, Kyle Lee, James Mulligan, Mateusz Płoskoń, Felix Ringer, and Xiaojun Yao, “Quantum simulation of nonequilibrium dynamics and thermalization in the Schwinger model,” *Phys. Rev. D* **106**, 054508 (2022), arXiv:2106.08394 [quant-ph].
- [36] Kyle Lee, James Mulligan, Felix Ringer, and Xiaojun Yao, “Liouvillian Dynamics of the Open Schwinger Model: String Breaking and Kinetic Dissipation in a Thermal Medium,” (2023), arXiv:2308.03878 [quant-ph].
- [37] Adrien Florio, David Frenklakh, Kazuki Ikeda, Dmitri Kharzeev, Vladimir Korepin, Shuzhe Shi, and Kwangmin Yu, “Real-Time Nonperturbative Dynamics of Jet Production in Schwinger Model: Quantum Entanglement and Vacuum Modification,” *Phys. Rev. Lett.* **131**, 021902 (2023), arXiv:2301.11991 [hep-ph].
- [38] T. V. Zache, N. Mueller, J. T. Schneider, F. Jendrzejewski, J. Berges, and P. Hauke, “Dynamical Topological Transitions in the Massive Schwinger Model

- with a θ Term,” *Phys. Rev. Lett.* **122**, 050403 (2019), arXiv:1808.07885 [quant-ph].
- [39] Dmitri E. Kharzeev and Yuta Kikuchi, “Real-time chiral dynamics from a digital quantum simulation,” *Phys. Rev. Res.* **2**, 023342 (2020), arXiv:2001.00698 [hep-ph].
- [40] Kazuki Ikeda, Dmitri E. Kharzeev, and Yuta Kikuchi, “Real-time dynamics of Chern-Simons fluctuations near a critical point,” *Phys. Rev. D* **103**, L071502 (2021), arXiv:2012.02926 [hep-ph].
- [41] Edward Witten, “Baryons in the $1/n$ Expansion,” *Nucl. Phys. B* **160**, 57–115 (1979).
- [42] Paul J. Steinhardt, “Baryons and Baryonium in QCD in Two-dimensions,” *Nucl. Phys. B* **176**, 100–112 (1980).
- [43] Barak Bringoltz, “Solving two-dimensional large- N QCD with a nonzero density of baryons and arbitrary quark mass,” *Phys. Rev. D* **79**, 125006 (2009), arXiv:0901.4035 [hep-lat].
- [44] Marton Lajer, Robert M. Konik, Robert D. Pisarski, and Alexei M. Tsvelik, “When cold, dense quarks in 1+1 and 3+1 dimensions are not a Fermi liquid,” *Phys. Rev. D* **105**, 054035 (2022), arXiv:2112.10238 [hep-th].
- [45] E. Rico, M. Dalmonte, P. Zoller, D. Banerjee, M. Bögli, P. Stebler, and U. J. Wiese, “ $SO(3)$ Nuclear Physics” with ultracold Gases,” *Annals Phys.* **393**, 466–483 (2018), arXiv:1802.00022 [cond-mat.quant-gas].
- [46] Roland C. Farrell, Ivan A. Chernyshev, Sarah J. M. Powell, Nikita A. Zemlevskiy, Marc Illa, and Martin J. Savage, “Preparations for quantum simulations of quantum chromodynamics in 1+1 dimensions. I. Axial gauge,” *Phys. Rev. D* **107**, 054512 (2023), arXiv:2207.01731 [quant-ph].
- [47] Jean-Loup Gervais and B. Sakita, “Gauge degrees of freedom, external charges, quark confinement criterion in $A_0 = 0$ canonical formalism,” *Phys. Rev. D* **18**, 453 (1978).
- [48] Robert D. Pisarski, “Wilson loops in the Hamiltonian formalism,” *Phys. Rev. D* **105**, L111501 (2022), arXiv:2202.11122 [hep-th].
- [49] David E. Kaplan, Tom Melia, and Surjeet Rajendran, “The Classical Equations of Motion of Quantized Gauge Theories, Part 2: Electromagnetism,” (2023), arXiv:2307.09475 [hep-th].
- [50] Adrian Dumitru, Robert D. Pisarski, and Detlef Zschiesche, “Dense quarks, and the fermion sign problem, in a $SU(N)$ matrix model,” *Phys. Rev. D* **72**, 065008 (2005), arXiv:hep-ph/0505256.
- [51] R. Narayanan, “Two flavor massless Schwinger model on a torus at a finite chemical potential,” *Phys. Rev. D* **86**, 125008 (2012), arXiv:1210.3072 [hep-th].
- [52] Robert Lohmayer and Rajamani Narayanan, “Phase structure of two-dimensional QED at zero temperature with flavor-dependent chemical potentials and the role of multidimensional theta functions,” *Phys. Rev. D* **88**, 105030 (2013), arXiv:1307.4969 [hep-th].
- [53] Mari Carmen Bañuls, Krzysztof Cichy, J. Ignacio Cirac, Karl Jansen, and Stefan Kühn, “Density Induced Phase Transitions in the Schwinger Model: A Study with Matrix Product States,” *Phys. Rev. Lett.* **118**, 071601 (2017), arXiv:1611.00705 [hep-lat].
- [54] Robert D. Pisarski, “Remarks on nuclear matter: How an ω_0 condensate can spike the speed of sound, and a model of $Z(3)$ baryons,” *Phys. Rev. D* **103**, L071504 (2021), arXiv:2101.05813 [nucl-th].
- [55] Andreas Weichselbaum, “Non-abelian symmetries in tensor networks: A quantum symmetry space approach,” *Annals of Physics* **327**, 2972–3047 (2012).
- [56] Roman Orus, “A Practical Introduction to Tensor Networks: Matrix Product States and Projected Entangled Pair States,” *Annals Phys.* **349**, 117–158 (2014), arXiv:1306.2164 [cond-mat.str-el].
- [57] Matthew Fishman, Steven R. White, and E. Miles Stoudenmire, “The ITensor Software Library for Tensor Network Calculations,” (2020), 10.21468/SciPost-PhysCodeb.4, arXiv:2007.14822 [cs.MS].
- [58] Yannick Meurice, Ryo Sakai, and Judah Unmuth-Yockey, “Tensor lattice field theory for renormalization and quantum computing,” *Rev. Mod. Phys.* **94**, 025005 (2022), arXiv:2010.06539 [hep-lat].
- [59] Jeff Greensite, “Confinement from Center Vortices: A review of old and new results,” *EPJ Web Conf.* **137**, 01009 (2017), arXiv:1610.06221 [hep-lat].
- [60] Nicholas Sale, Biagio Lucini, and Jeffrey Giansiracusa, “Probing center vortices and deconfinement in $SU(2)$ lattice gauge theory with persistent homology,” *Phys. Rev. D* **107**, 034501 (2023), arXiv:2207.13392 [hep-lat].
- [61] James C. Biddle, Waseem Kamleh, and Derek B. Leinweber, “Static quark potential from center vortices in the presence of dynamical fermions,” *Phys. Rev. D* **106**, 054505 (2022), arXiv:2206.00844 [hep-lat].
- [62] James C. Biddle, Waseem Kamleh, and Derek B. Leinweber, “Impact of dynamical fermions on the center vortex gluon propagator,” *Phys. Rev. D* **106**, 014506 (2022), arXiv:2206.02320 [hep-lat].
- [63] James C. Biddle, Waseem Kamleh, and Derek B. Leinweber, “Center vortex structure in the presence of dynamical fermions,” *Phys. Rev. D* **107**, 094507 (2023), arXiv:2302.05897 [hep-lat].
- [64] D. Horn, M. Weinstein, and S. Yankielowicz, “HAMILTONIAN APPROACH TO $Z(N)$ LATTICE GAUGE THEORIES,” *Phys. Rev. D* **19**, 3715 (1979).
- [65] J. B. Kogut, R. B. Pearson, J. Shigemitsu, and D. K. Sinclair, “ $Z(N)$ and N State Potts Lattice Gauge Theories: Phase Diagrams, First Order Transitions, Beta Functions and $1/N$ Expansions,” *Phys. Rev. D* **22**, 2447 (1980).
- [66] John B. Kogut, “ $1/n$ Expansions and the Phase Diagram of Discrete Lattice Gauge Theories With Matter Fields,” *Phys. Rev. D* **21**, 2316 (1980).
- [67] F. C. Alcaraz and R. Koberle, “The Phases of Two-dimensional Spin and Four-dimensional Gauge Systems With $Z(N)$ Symmetry,” *J. Phys. A* **14**, 1169 (1981).
- [68] F. C. Alcaraz and R. Koberle, “Duality and the Phases of $Z(n)$ Spin Systems,” *J. Phys. A* **13**, L153 (1980).
- [69] Erez Zohar, Alessandro Farace, Benni Reznik, and J. Ignacio Cirac, “Digital lattice gauge theories,” *Phys. Rev. A* **95**, 023604 (2017), arXiv:1607.08121 [quant-ph].
- [70] Elisa Ercolessi, Paolo Facchi, Giuseppe Magnifico, Saverio Pascazio, and Francesco V. Pepe, “Phase Transitions in Z_n Gauge Models: Towards Quantum Simulations of the Schwinger-Weyl QED,” *Phys. Rev. D* **98**, 074503 (2018), arXiv:1705.11047 [quant-ph].
- [71] G. Magnifico, D. Vodola, E. Ercolessi, S. P. Kumar, M. Müller, and A. Bermudez, “Symmetry-protected topological phases in lattice gauge theories: topological QED₂,” *Phys. Rev. D* **99**, 014503 (2019), arXiv:1804.10568 [cond-mat.quant-gas].
- [72] G. Magnifico, D. Vodola, E. Ercolessi, S. P. Kumar, M. Müller, and A. Bermudez, “ Z_N gauge theories cou-

- pled to topological fermions: QED₂ with a quantum-mechanical θ angle,” Phys. Rev. B **100**, 115152 (2019), arXiv:1906.07005 [cond-mat.quant-gas].
- [73] Umberto Borla, Ruben Verresen, Fabian Grusdt, and Sergej Moroz, “Confined Phases of One-Dimensional Spinless Fermions Coupled to Z_2 Gauge Theory,” Phys. Rev. Lett. **124**, 120503 (2020), arXiv:1909.07399 [cond-mat.str-el].
- [74] Jernej Frank, Emilie Huffman, and Shailesh Chandrasekharan, “Emergence of Gauss’ law in a Z_2 lattice gauge theory in $1 + 1$ dimensions,” Phys. Lett. B **806**, 135484 (2020), arXiv:1904.05414 [cond-mat.str-el].
- [75] Patrick Emonts, Mari Carmen Bañuls, Ignacio Cirac, and Erez Zohar, “Variational Monte Carlo simulation with tensor networks of a pure Z_3 gauge theory in $(2+1)d$,” Phys. Rev. D **102**, 074501 (2020), arXiv:2008.00882 [quant-ph].
- [76] Daniel Robaina, Mari Carmen Bañuls, and J. Ignacio Cirac, “Simulating $2+1D$ Z_3 Lattice Gauge Theory with an Infinite Projected Entangled-Pair State,” Phys. Rev. Lett. **126**, 050401 (2021), arXiv:2007.11630 [hep-lat].
- [77] Patrick Emonts, Ariel Kelman, Umberto Borla, Sergej Moroz, Snir Gazit, and Erez Zohar, “Finding the ground state of a lattice gauge theory with fermionic tensor networks: A $2+1D$ Z_2 demonstration,” Phys. Rev. D **107**, 014505 (2023), arXiv:2211.00023 [quant-ph].
- [78] S. Chandrasekharan and U. J. Wiese, “Quantum link models: A Discrete approach to gauge theories,” Nucl. Phys. B **492**, 455–474 (1997), arXiv:hep-lat/9609042.
- [79] R. Brower, S. Chandrasekharan, and U. J. Wiese, “QCD as a quantum link model,” Phys. Rev. D **60**, 094502 (1999), arXiv:hep-th/9704106.
- [80] Bipasha Chakraborty, Masazumi Honda, Taku Izubuchi, Yuta Kikuchi, and Akio Tomiya, “Classically emulated digital quantum simulation of the Schwinger model with a topological term via adiabatic state preparation,” Phys. Rev. D **105**, 094503 (2022), arXiv:2001.00485 [hep-lat].
- [81] Lawrence M. Krauss and Frank Wilczek, “Discrete Gauge Symmetry in Continuum Theories,” Phys. Rev. Lett. **62**, 1221 (1989).
- [82] John Preskill and Lawrence M. Krauss, “Local Discrete Symmetry and Quantum Mechanical Hair,” Nucl. Phys. B **341**, 50–100 (1990).
- [83] Andreas Weichselbaum, “Non-abelian symmetries in tensor networks: A quantum symmetry space approach,” Annals of Physics **327**, 2972 – 3047 (2012).
- [84] W. P. Su, J. R. Schrieffer, and A. J. Heeger, “Solitons in polyacetylene,” Phys. Rev. Lett. **42**, 1698–1701 (1979).
- [85] Navketan Batra and Goutam Sheet, “Physics with coffee and doughnuts,” Resonance **25**, 765–786 (2020).
- [86] Ziteng Wang, Xiangdong Wang, Zhichan Hu, Domenico Bongiovanni, Dario Jukić, Liqin Tang, Daohong Song, Roberto Morandotti, Zhigang Chen, and Hrvoje Buljan, “Sub-symmetry-protected topological states,” Nature Physics **19**, 992–998 (2023).
- [87] DLMF, “NIST Digital Library of Mathematical Functions,” <https://dlmf.nist.gov/>, Release 1.1.11 of 2023-09-15, f. W. J. Olver, A. B. Olde Daalhuis, D. W. Lozier, B. I. Schneider, R. F. Boisvert, C. W. Clark, B. R. Miller, B. V. Saunders, H. S. Cohl, and M. A. McClain, eds.
- [88] Andreas Weichselbaum, “X-symbols for non-abelian symmetries in tensor networks,” Phys. Rev. Research **2**, 023385 (2020).
- [89] Andreas Weichselbaum, “QSpace tensor library (v4.0),” <https://bitbucket.org/qspace4u/> (2006-2023).
- [90] Alfred Young, “On quantitative substitutional analysis,” Proceedings of the London Mathematical Society, 556–556 (1930).
- [91] Robert N Cahn, *Semi-simple Lie algebras and their representations* (The Benjamin/Cummings Publishing Company, 1984).
- [92] Steven R. White, “Density matrix formulation for quantum renormalization groups,” Phys. Rev. Lett. **69**, 2863–2866 (1992).
- [93] Ulrich Schollwöck, “The density-matrix renormalization group in the age of matrix product states,” Ann. Phys. **326**, 96–192 (2011).
- [94] Rajesh Kumar et al. (MUSES), “Theoretical and Experimental Constraints for the Equation of State of Dense and Hot Matter,” (2023), arXiv:2303.17021 [nucl-th].
- [95] Tim Dietrich, Michael W. Coughlin, Peter T. H. Pang, Mattia Bulla, Jack Heinzl, Lina Issa, Ingo Tews, and Sarah Antier, “Multimessenger constraints on the neutron-star equation of state and the Hubble constant,” Science **370**, 1450–1453 (2020), arXiv:2002.11355 [astro-ph.HE].
- [96] Szabolcs Borsanyi, Zoltan Fodor, Jana N. Guenther, Ruben Kara, Sandor D. Katz, Paolo Parotto, Attila Pasztor, Claudia Ratti, and Kalman K. Szabo, “QCD Crossover at Finite Chemical Potential from Lattice Simulations,” Phys. Rev. Lett. **125**, 052001 (2020), arXiv:2002.02821 [hep-lat].
- [97] D. Bollweg, J. Goswami, O. Kaczmarek, F. Karsch, Swagato Mukherjee, P. Petreczky, C. Schmidt, and P. Scior (HotQCD), “Taylor expansions and Padé approximants for cumulants of conserved charge fluctuations at nonvanishing chemical potentials,” Phys. Rev. D **105**, 074511 (2022), arXiv:2202.09184 [hep-lat].
- [98] D. Bollweg, D. A. Clarke, J. Goswami, O. Kaczmarek, F. Karsch, Swagato Mukherjee, P. Petreczky, C. Schmidt, and Sipaz Sharma (HotQCD), “Equation of state and speed of sound of $(2+1)$ -flavor QCD in strangeness-neutral matter at nonvanishing net baryon-number density,” Phys. Rev. D **108**, 014510 (2023), arXiv:2212.09043 [hep-lat].
- [99] Sabarnya Mitra, Prasad Hegde, and Christian Schmidt, “New way to resum the lattice QCD Taylor series equation of state at finite chemical potential,” Phys. Rev. D **106**, 034504 (2022), arXiv:2205.08517 [hep-lat].
- [100] Sabarnya Mitra and Prasad Hegde, “QCD equation of state at finite chemical potential from an unbiased exponential resummation of the lattice QCD Taylor series,” Phys. Rev. D **108**, 034502 (2023), arXiv:2302.06460 [hep-lat].
- [101] Masahiro Ishii, Akihisa Miyahara, Hiroaki Kouno, and Masanobu Yahiro, “Extrapolation for meson screening masses from imaginary to real chemical potential,” Phys. Rev. D **99**, 114010 (2019), arXiv:1807.08110 [hep-ph].
- [102] A. Begun, V. G. Bornyakov, N. V. Gerasimeniuk, V. A. Goy, A. Nakamura, R. N. Rogalyov, and V. Vovchenko, “Quark Density in Lattice QCD₂D at Imaginary and Real Chemical Potential,” (2021), arXiv:2103.07442 [hep-lat].
- [103] V. G. Bornyakov, N. V. Gerasimeniuk, V. A. Goy, A. A. Korneev, A. V. Molochkov, A. Nakamura, and

- R. N. Rogalyov, “Numerical study of the Roberge-Weiss transition,” *Phys. Rev. D* **107**, 014508 (2023), arXiv:2203.06159 [hep-lat].
- [104] Bastian B. Brandt, Amine Chabane, Volodymyr Chelnokov, Francesca Cuteri, Gergely Endrődi, and Christopher Winterowd, “The light Roberge-Weiss tricritical endpoint at imaginary isospin and baryon chemical potential,” (2022), arXiv:2207.10117 [hep-lat].
- [105] Szabolcs Borsanyi, Zoltan Fodor, Matteo Giordano, Sandor D. Katz, Daniel Negradi, Attila Pasztor, and Chik Him Wong, “Lattice simulations of the QCD chiral transition at real baryon density,” *Phys. Rev. D* **105**, L051506 (2022), arXiv:2108.09213 [hep-lat].
- [106] Szabolcs Borsanyi, Zoltan Fodor, Matteo Giordano, Jana N. Guenther, Sandor D. Katz, Attila Pasztor, and Chik Him Wong, “Equation of state of a hot-and-dense quark gluon plasma: Lattice simulations at real μB vs extrapolations,” *Phys. Rev. D* **107**, L091503 (2023), arXiv:2208.05398 [hep-lat].
- [107] Giuseppe Gagliardi and Wolfgang Unger, “New dual representation for staggered lattice QCD,” *Phys. Rev. D* **101**, 034509 (2020), arXiv:1911.08389 [hep-lat].
- [108] Owe Philipsen and Jonas Scheunert, “QCD in the heavy dense regime for general N_c : on the existence of quarkyonic matter,” *JHEP* **11**, 022 (2019), arXiv:1908.03136 [hep-lat].
- [109] Jangho Kim, Anh Quang Pham, Owe Philipsen, and Jonas Scheunert, “The SU(3) spin model with chemical potential by series expansion techniques,” *JHEP* **10**, 051 (2020), arXiv:2007.04187 [hep-lat].
- [110] Marc Klegrewe and Wolfgang Unger, “Strong Coupling Lattice QCD in the Continuous Time Limit,” *Phys. Rev. D* **102**, 034505 (2020), arXiv:2005.10813 [hep-lat].
- [111] Owe Philipsen, “Lattice Constraints on the QCD Chiral Phase Transition at Finite Temperature and Baryon Density,” *Symmetry* **13**, 2079 (2021), arXiv:2111.03590 [hep-lat].
- [112] Owe Philipsen, “Strong coupling methods in QCD thermodynamics,” *Indian J. Phys.* **95**, 1599–1611 (2021), arXiv:2104.03696 [hep-lat].
- [113] Jangho Kim, Pratitee Pattanaik, and Wolfgang Unger, “Nuclear liquid-gas transition in the strong coupling regime of lattice QCD,” *Phys. Rev. D* **107**, 094514 (2023), arXiv:2303.01467 [hep-lat].
- [114] J. B. Kogut and D. K. Sinclair, “Applying Complex Langevin Simulations to Lattice QCD at Finite Density,” *Phys. Rev. D* **100**, 054512 (2019), arXiv:1903.02622 [hep-lat].
- [115] Dénes Sexty, “Calculating the equation of state of dense quark-gluon plasma using the complex Langevin equation,” *Phys. Rev. D* **100**, 074503 (2019), arXiv:1907.08712 [hep-lat].
- [116] Yuta Ito, Hideo Matsufuru, Yusuke Namekawa, Jun Nishimura, Shinji Shimasaki, Asato Tsuchiya, and Shoichiro Tsutsui, “Complex Langevin calculations in QCD at finite density,” *JHEP* **10**, 144 (2020), arXiv:2007.08778 [hep-lat].
- [117] Erhard Seiler, Dénes Sexty, and Ion-Olimpiu Stamatescu, “Complex Langevin: Correctness criteria, boundary terms and spectrum,” (2023), arXiv:2304.00563 [hep-lat].
- [118] Philipp Isserstedt, Michael Buballa, Christian S. Fischer, and Pascal J. Gunkel, “Baryon number fluctuations in the QCD phase diagram from Dyson-Schwinger equations,” *Phys. Rev. D* **100**, 074011 (2019), arXiv:1906.11644 [hep-ph].
- [119] Pascal J. Gunkel and Christian S. Fischer, “Locating the critical endpoint of QCD: Mesonic backcoupling effects,” *Phys. Rev. D* **104**, 054022 (2021), arXiv:2106.08356 [hep-ph].
- [120] Julian Bernhardt, Christian S. Fischer, Philipp Isserstedt, and Bernd-Jochen Schaefer, “Critical endpoint of QCD in a finite volume,” *Phys. Rev. D* **104**, 074035 (2021), arXiv:2107.05504 [hep-ph].
- [121] Fei Gao and Jan M. Pawłowski, “QCD phase structure from functional methods,” *Phys. Rev. D* **102**, 034027 (2020), arXiv:2002.07500 [hep-ph].
- [122] N. Dupuis, L. Canet, A. Eichhorn, W. Metzner, J. M. Pawłowski, M. Tissier, and N. Wschebor, “The nonperturbative functional renormalization group and its applications,” *Phys. Rept.* **910**, 1–114 (2021), arXiv:2006.04853 [cond-mat.stat-mech].
- [123] Philipp Isserstedt, Christian S. Fischer, and Thorsten Steinert, “Thermodynamics from the quark condensate,” *Phys. Rev. D* **103**, 054012 (2021), arXiv:2012.04991 [hep-ph].
- [124] Wei-jie Fu, Xiaofeng Luo, Jan M. Pawłowski, Fabian Rennecke, Rui Wen, and Shi Yin, “Hyper-order baryon number fluctuations at finite temperature and density,” *Phys. Rev. D* **104**, 094047 (2021), arXiv:2101.06035 [hep-ph].
- [125] Yong-rui Chen, Rui Wen, and Wei-jie Fu, “Critical behaviors of the O(4) and Z(2) symmetries in the QCD phase diagram,” *Phys. Rev. D* **104**, 054009 (2021), arXiv:2101.08484 [hep-ph].
- [126] Alejandro Ayala, Bilgai Almeida Zamora, J. J. Cobos-Martínez, S. Hernández-Ortiz, L. A. Hernández, Alfredo Raya, and María Elena Tejada-Yeomans, “Collision energy dependence of the critical end point from baryon number fluctuations in the Linear Sigma Model with quarks,” *Eur. Phys. J. A* **58**, 87 (2022), arXiv:2108.02362 [hep-ph].
- [127] Wei-jie Fu, “QCD at finite temperature and density within the fRG approach: an overview,” *Commun. Theor. Phys.* **74**, 097304 (2022), arXiv:2205.00468 [hep-ph].
- [128] Konstantin Otto, Christopher Busch, and Bernd-Jochen Schaefer, “Regulator scheme dependence of the chiral phase transition at high densities,” *Phys. Rev. D* **106**, 094018 (2022), arXiv:2206.13067 [hep-ph].
- [129] Wei-jie Fu, Xiaofeng Luo, Jan M. Pawłowski, Fabian Rennecke, and Shi Yin, “Ripples of the QCD Critical Point,” (2023), arXiv:2308.15508 [hep-ph].
- [130] Julian Bernhardt and Christian S. Fischer, “From imaginary to real chemical potential QCD with functional methods,” *Eur. Phys. J. A* **59**, 181 (2023), arXiv:2305.01434 [hep-ph].
- [131] Matthew Fishman, Steven R. White, and E. Miles Stoudenmire, “The ITensor Software Library for Tensor Network Calculations,” *SciPost Phys. Codebases*, 4 (2022).
- [132] Matthew Fishman, Steven R. White, and E. Miles Stoudenmire, “Codebase release 0.3 for ITensor,” *SciPost Phys. Codebases*, 4–r0.3 (2022).
- [133] Thomas D. Cohen, “QCD functional integrals for systems with nonzero chemical potential,” in *From Fields to Strings: Circumnavigating Theoretical Physics: A C* (2004) pp. 101–120, arXiv:hep-ph/0405043.

- [134] Gert Aarts, “Introductory lectures on lattice QCD at nonzero baryon number,” *J. Phys. Conf. Ser.* **706**, 022004 (2016), arXiv:1512.05145 [hep-lat].